Supplement of Atmos. Chem. Phys., 25, 15343–15357, 2025
https://doi.org/10.5194/acp-25-15343-2025-supplement
© Author(s) 2025. CC BY 4.0 License.

Atmospheric Chemistry and Physics
Open Access
EGU

*Supplement of*

# Deciphering dust provenance and transport pathways across Northern China's source-sink systems

**Lanying Han et al.**

*Correspondence to:* Zhengcai Zhang (zhangzhengcai@snnu.edu.cn)

The copyright of individual parts of the supplement might differ from the article licence.

Table S1 The most popular geochemical fingerprinting indices used to identify dust provenance in northern China.

| Indexes | Regions | References |
|---|---|---|
| Eu/Eu*, $(Gd/Yb)_n$, $(La/Yb)_n$, $(La/Sm)_n$ | Qilian Mountains | Wei et al. (2017) |
| Eu/Eu* | Northern China | Chen et al. (2017) |
| Eu/Eu*, Y/ΣREE, La/Er, La/Gd, Gd/Er, La/Yb, Y/Tb, Y/La, Y/Nd, La/Th | Northern China | Ferrat et al. (2011) |
| Eu/Eu*, $(La/Yb)_n$, $(La/Sm)_n$, $(Gd/Yb)_n$ | Northeastern China | Xie and Chi (2016) |
| $(La/Yb)_n$ | Northern China | Yang et al. (2007) |
| Eu/Eu*, $(La/Yb)_n$ | Chinese Loess Plateau | Jahn et al. (2001) |
| Eu/Eu*, $(Gd/Yb)_n$, $(La/Sm)_n$ | Chinese Loess Plateau | Ding et al. (2001) |
| Eu/Eu*, $(La/Yb)_n$, La/Th | Chinese Loess Plateau | Gallet et al. (1996) |
| Th/Sc, La/Th | Chinese Loess Plateau | Liu et al. (1993) |

Table S2 Main climate and related conditions at the meteorological station sites in the study region. Their locations are shown in Figure S1. *DP* is the drift potential in vector units and *RDD* is the resultant drift direction; they were calculated using the methods of Fryberger and Dean (1979). $U_{mean}$, mean annual wind speed; *MAT*, mean annual temperature. High *DP* indicates strong wind erosion in the dust source region and strong transport of dust material to transitional regions (such as the Tengger Desert) and downwind regions (such as the Chinese Loess Plateau).

| | Karamay | Hongliuhe | Mazun | Ejina | Hongsan | Zhongwei | Yulin |
|---|---|---|---|---|---|---|---|
| Elevation (m asl) | 500 | 2692 | 2200 | 910 | 1329 | 1307 | 1100 |
| Total annual rainfall (mm) | 105 | 45.5 | 150 | 37 | 70 | 94 | 438 |
| *MAT* (°C) | 8.6 | 11.4 | 6.3 | 8.3 | 9 | 12 | 8.1 |
| $U_{mean}$ (m $s^{-1}$) | 3.70 | 4.05 | 4.19 | 2.9 | 3.9 | 2.6 | 3.6 |
| *DP* (VU) | 475 | 268 | 348 | 91 | 405[a] | 69[b] | 70[c] |
| *RDD* (°) | 312 | 76 | 339 | 297 | 317[a] | 303[b] | 311[c] |

[a] Data from Hongsan are from Zhang et al., 2015; [b] Data from Zhongwei are from Dong et al. (2014); [c] Data from Yulin are from Liu and Yang (2018).

Table S3 The composition of trace elements and rare earth elements at the 40 sample sites. Site abbreviations: A, Alxa Plateau; C, Hexi Corridor and its adjacent region; G, Guerbantonggute Desert; H, Heihe River Basin; L, Lanzhou; M, Mu Us Desert; Q, Qaidam Basin; T, Tengger Desert.

| | | G1 | G2 | G3 | G4 | G5 | G6 | G7 | Q1 | Q2 | Q3 | Q4 | Q5 | A1 | A2 | A3 | A4 | A5 |
|---|---|---|---|---|---|---|---|---|---|---|---|---|---|---|---|---|---|---|
| Trace elements (μg/g) | Sc | 13.7 | 15.9 | 14.1 | 11.7 | 14.8 | 16.8 | 13.4 | 10.8 | 11.7 | 15.4 | 12.8 | 16.8 | 13.8 | 8.75 | 16.3 | 15.8 | 19 |
| | Rb | 112 | 87.1 | 126 | 108 | 132 | 121 | 122 | 115 | 83.5 | 109 | 71.8 | 105 | 135 | 89.7 | 93.1 | 113 | 103 |
| | Sr | 264 | 261 | 401 | 420 | 286 | 239 | 610 | 271 | 356 | 340 | 90.6 | 123 | 304 | 298 | 322 | 314 | 316 |
| | Y | 33.6 | 49.6 | 29.8 | 29.8 | 29.7 | 28.7 | 26.4 | 27.6 | 38.5 | 34.5 | 31.2 | 42 | 26.6 | 20.1 | 32 | 37.2 | 36.3 |
| | Zr | 233 | 359 | 179 | 150 | 218 | 164 | 179 | 389 | 315 | 290 | 166 | 223 | 232 | 210 | 316 | 395 | 254 |
| | Nb | 11 | 15.4 | 10.6 | 9.21 | 11.4 | 10.9 | 9.03 | 15.4 | 14.4 | 15.8 | 18.9 | 15.5 | 12.6 | 7.32 | 13.5 | 17.8 | 11.5 |
| | Ba | 522 | 375 | 539 | 563 | 493 | 427 | 480 | 539 | 489 | 575 | 3.52 | 6.43 | 637 | 780 | 600 | 609 | 478 |
| | Hf | 6.33 | 10.1 | 4.81 | 4 | 5.77 | 4.47 | 4.82 | 10.4 | 8.79 | 8.11 | 4.78 | 5.74 | 6.17 | 5.31 | 8.56 | 10.4 | 6.8 |
| | Ta | 0.892 | 1.47 | 0.82 | 0.771 | 0.953 | 0.887 | 0.716 | 1.25 | 1.25 | 1.29 | 4.83 | 4.24 | 1.08 | 1.05 | 1.13 | 1.76 | 0.89 |
| | Pb | 19.9 | 20.2 | 23.5 | 19.7 | 22.3 | 16.9 | 19 | 21 | 13.9 | 23.7 | 32.3 | 5.27 | 21.4 | 15.6 | 19.2 | 25.7 | 22.9 |
| | Th | 11.2 | 14.7 | 11.6 | 13.1 | 12.2 | 10.6 | 9.67 | 25.2 | 11.9 | 13.6 | 14.1 | 25.1 | 17.1 | 6.35 | 8.59 | 15.7 | 11.5 |
| Rare earth elements (μg/g) | La | 31.6 | 45 | 30.5 | 34.4 | 35.6 | 28.4 | 25 | 35.5 | 38.2 | 39.4 | 20.2 | 27.6 | 34.3 | 23.9 | 39.4 | 18.7 | 25.9 |
| | Ce | 68 | 97.7 | 65.5 | 74.4 | 78.2 | 64.8 | 52 | 76.5 | 80.8 | 83.7 | 39.2 | 52.5 | 73.9 | 49.1 | 83.7 | 37.3 | 57.6 |
| | Pr | 7.98 | 11.2 | 7.56 | 8.65 | 8.91 | 7.25 | 6.22 | 9.17 | 9.26 | 9.66 | 4.5 | 6.34 | 8.79 | 5.58 | 9.54 | 4.46 | 6.82 |
| | Nd | 31.4 | 44.3 | 29.9 | 34.2 | 34.8 | 28.9 | 24.6 | 35.6 | 34.9 | 37.4 | 17.2 | 24 | 34.9 | 21.5 | 36.4 | 17.3 | 27.6 |
| | Sm | 6.36 | 9.41 | 6 | 7.01 | 7.01 | 5.95 | 5.05 | 6.98 | 6.55 | 7.56 | 3.33 | 4.85 | 7.22 | 4.31 | 7.01 | 3.6 | 5.93 |
| | Eu | 1.34 | 1.68 | 1.26 | 1.34 | 1.35 | 1.31 | 1.06 | 1.17 | 1.2 | 1.48 | 0.66 | 0.91 | 1.49 | 0.94 | 1.18 | 0.84 | 1.31 |
| | Gd | 5.83 | 8.73 | 5.5 | 6.02 | 5.65 | 5.16 | 4.44 | 5.58 | 5.76 | 6.51 | 2.96 | 4.06 | 6.39 | 3.73 | 5.53 | 3.23 | 5.39 |
| | Tb | 0.91 | 1.39 | 0.84 | 0.93 | 0.87 | 0.82 | 0.72 | 0.84 | 0.96 | 1.02 | 0.46 | 0.64 | 1.03 | 0.59 | 0.84 | 0.54 | 0.87 |
| | Dy | 5.46 | 8.19 | 4.93 | 5.22 | 4.96 | 4.8 | 4.34 | 4.8 | 6.15 | 5.99 | 2.73 | 3.8 | 6.27 | 3.45 | 4.68 | 3.3 | 5.28 |
| | Ho | 1.14 | 1.68 | 1.02 | 1.02 | 1.02 | 0.98 | 0.91 | 0.96 | 1.3 | 1.21 | 0.56 | 0.77 | 1.26 | 0.72 | 0.92 | 0.7 | 1.1 |
| | Er | 3.24 | 4.81 | 2.9 | 2.81 | 2.91 | 2.77 | 2.59 | 2.75 | 3.77 | 3.4 | 1.6 | 2.13 | 3.58 | 2.03 | 2.61 | 2.05 | 3.14 |
| | Tm | 0.48 | 0.7 | 0.41 | 0.4 | 0.42 | 0.4 | 0.38 | 0.4 | 0.55 | 0.49 | 0.23 | 0.31 | 0.52 | 0.3 | 0.37 | 0.3 | 0.46 |

| | | | | | | | | | | | | | | | | | | |
|---|---|---|---|---|---|---|---|---|---|---|---|---|---|---|---|---|---|---|
| | Yb | 3.18 | 4.85 | 2.76 | 2.6 | 2.87 | 2.68 | 2.58 | 2.81 | 3.59 | 3.36 | 1.55 | 2.05 | 3.46 | 2.01 | 2.54 | 2.08 | 3.14 |
| | Lu | 0.48 | 0.74 | 0.42 | 0.39 | 0.43 | 0.41 | 0.39 | 0.43 | 0.53 | 0.51 | 0.24 | 0.31 | 0.52 | 0.3 | 0.38 | 0.32 | 0.48 |
| | | A6 | A7 | C1 | C2 | C3 | C4 | C5 | C6 | C7 | C8 | H1 | H2 | H3 | H4 | H5 | H6 | H7 |
| Trace elements (μg/g) | Sc | 12.1 | 11.1 | 18.7 | 16.1 | 12.3 | 12.2 | 13.1 | 14.5 | 10.9 | 10.2 | 16.6 | 15.4 | 16.9 | 15.1 | 13.3 | 12.1 | 11.7 |
| | Rb | 102 | 107 | 105 | 97.5 | 122 | 83.6 | 79.7 | 70.9 | 94.9 | 94 | 100 | 99.2 | 165 | 86.7 | 118 | 101 | 102 |
| | Sr | 274 | 236 | 307 | 261 | 257 | 246 | 260 | 263 | 234 | 230 | 256 | 257 | 277 | 270 | 344 | 227 | 240 |
| | Y | 32.7 | 27.1 | 36.8 | 42.8 | 27.9 | 28.6 | 35.1 | 40.6 | 20.7 | 20.3 | 31.1 | 37.8 | 26 | 42.9 | 23.7 | 23.8 | 30.2 |
| | Zr | 369 | 454 | 222 | 206 | 254 | 423 | 642 | 847 | 218 | 199 | 328 | 785 | 120 | 577 | 179 | 204 | 207 |
| | Nb | 13.9 | 13.7 | 12.1 | 10.3 | 13.4 | 13.2 | 15.3 | 19.4 | 10.7 | 9.88 | 19.7 | 22.9 | 12.6 | 16.2 | 11.3 | 12.4 | 11.5 |
| | Ba | 674 | 596 | 472 | 473 | 523 | 538 | 527 | 432 | 883 | 1532 | 912 | 642 | 649 | 543 | 640 | 585 | 601 |
| | Hf | 10.1 | 12.2 | 5.64 | 5.48 | 6.64 | 11.1 | 16.5 | 22.1 | 5.49 | 5.47 | 8.92 | 20.9 | 3.28 | 15.7 | 4.65 | 5.43 | 5.66 |
| | Ta | 1.07 | 1.13 | 0.926 | 0.82 | 1.19 | 1.35 | 1.57 | 2.11 | 0.792 | 0.838 | 1.5 | 2.23 | 0.952 | 1.44 | 0.853 | 1.2 | 0.887 |
| | Pb | 18.3 | 20.8 | 22.3 | 33.9 | 20.1 | 17.3 | 17.5 | 17.7 | 43.2 | 27.7 | 22.3 | 21.4 | 27.2 | 23.2 | 23.9 | 16.6 | 17.1 |
| | Th | 12.5 | 18.8 | 10.7 | 11.9 | 14.4 | 11.5 | 14.3 | 17 | 8.7 | 8.28 | 28 | 22.7 | 14.8 | 21.6 | 11.9 | 10.2 | 11.3 |
| Rare earth elements (μg/g) | La | 48.8 | 41.8 | 44.1 | 32.2 | 33.4 | 30.7 | 32.8 | 48.1 | 23.5 | 29 | 33.5 | 34.6 | 38.9 | 32.9 | 50.6 | 54.2 | 35 |
| | Ce | 107 | 91.8 | 91 | 70.1 | 73.7 | 63.9 | 68.7 | 101 | 47.6 | 57.7 | 72.6 | 79.8 | 85.4 | 69 | 107 | 119 | 74.2 |
| | Pr | 12.3 | 10.5 | 10.7 | 8.47 | 8.59 | 7.21 | 7.66 | 11.9 | 5.54 | 6.5 | 8 | 9.37 | 9.6 | 7.81 | 11.6 | 13 | 8.37 |
| | Nd | 46.7 | 39.9 | 41 | 33.7 | 34 | 27 | 28.6 | 45 | 21.3 | 24.2 | 30.1 | 37.1 | 36 | 29.4 | 42.8 | 48.8 | 31.8 |
| | Sm | 9.03 | 7.73 | 8.01 | 7.09 | 7.17 | 5.08 | 5.43 | 9 | 4.15 | 4.55 | 5.84 | 7.66 | 7.06 | 5.67 | 7.8 | 9.11 | 6.11 |
| | Eu | 1.65 | 1.44 | 1.56 | 1.51 | 1.49 | 1.07 | 1.1 | 1.6 | 0.88 | 0.97 | 1.19 | 1.35 | 1.14 | 1.14 | 1.46 | 1.5 | 1.09 |
| | Gd | 7.5 | 6.53 | 6.73 | 6.37 | 6.69 | 4.47 | 4.75 | 7.96 | 3.62 | 4.01 | 4.95 | 5.97 | 5.76 | 5.02 | 6.39 | 7.49 | 5.06 |
| | Tb | 1.17 | 1.02 | 1.06 | 1.02 | 1.08 | 0.68 | 0.71 | 1.23 | 0.56 | 0.61 | 0.78 | 0.91 | 0.87 | 0.78 | 0.97 | 1.14 | 0.79 |
| | Dy | 6.81 | 5.94 | 6.23 | 6.12 | 6.84 | 3.97 | 4.07 | 7.18 | 3.23 | 3.57 | 4.49 | 5.28 | 4.8 | 4.69 | 5.46 | 6.4 | 4.47 |
| | Ho | 1.41 | 1.23 | 1.26 | 1.25 | 1.46 | 0.81 | 0.81 | 1.48 | 0.65 | 0.73 | 0.91 | 1.12 | 0.96 | 0.96 | 1.11 | 1.31 | 0.91 |
| | Er | 4.05 | 3.5 | 3.62 | 3.58 | 4.2 | 2.27 | 2.29 | 4.24 | 1.79 | 2.07 | 2.54 | 3.31 | 2.69 | 2.72 | 3.13 | 3.75 | 2.56 |
| | Tm | 0.6 | 0.51 | 0.53 | 0.53 | 0.61 | 0.32 | 0.33 | 0.62 | 0.26 | 0.3 | 0.36 | 0.51 | 0.39 | 0.4 | 0.45 | 0.55 | 0.37 |

| | | | | | | | | | | | | | | | | | |
|---|---|---|---|---|---|---|---|---|---|---|---|---|---|---|---|---|---|
| Yb | 4.15 | 3.52 | 3.59 | 3.54 | 4.1 | 2.17 | 2.21 | 4.27 | 1.68 | 2.01 | 2.43 | 3.52 | 2.77 | 2.66 | 2.99 | 3.86 | 2.48 |
| Lu | 0.64 | 0.53 | 0.55 | 0.54 | 0.61 | 0.33 | 0.33 | 0.65 | 0.25 | 0.3 | 0.37 | 0.55 | 0.43 | 0.41 | 0.46 | 0.61 | 0.37 |
| | H8 | H9 | H10 | M | T1 | T2 | T3 | L | K1 | K2 | K3 | K4 | K5 | K6 | K7 | | |
| Sc | 12 | 12.1 | 9.18 | 11 | 8.75 | 12.6 | 11.6 | 2.29 | 8.65 | 8.10 | 4.35 | 7.46 | 6.38 | 6.61 | 4.45 | | |
| Rb | 103 | 106 | 81.5 | 83.9 | 88.8 | 120 | 112 | 25.1 | 25.16 | 27.10 | 30.22 | 28.79 | 29.23 | 32.24 | 27.4 | | |
| Sr | 256 | 244 | 229 | 232 | 224 | 210 | 262 | 121 | 143.58 | 133.87 | 125.88 | 131.57 | 124.10 | 161.31 | 152.32 | | |
| Y | 27.5 | 24.7 | 18 | 26 | 19.5 | 26.4 | 26.3 | 35.6 | 20.27 | 24.55 | 13.33 | 12.49 | 14.07 | 13.89 | 11.58 | | |
| Zr | 254 | 223 | 124 | 326 | 187 | 234 | 309 | 268 | 132.03 | 650.10 | 62.21 | 73.99 | 91.22 | 96.49 | 116.46 | | |
| Nb | 12.4 | 11.1 | 8.84 | 10.7 | 9.86 | 12.3 | 11.8 | 15.6 | 10.98 | 8.98 | 5.85 | 6.55 | 6.95 | 6.54 | 4.96 | | |
| Ba | 631 | 670 | 532 | 449 | 599 | 644 | 627 | 758 | 345.89 | 268.32 | 236.94 | 275.71 | 242.17 | 220.31 | 198 | | |
| Hf | 6.83 | 5.75 | 3.18 | 8.66 | 4.8 | 5.98 | 8.18 | 6.74 | 4.72 | 19.59 | 2.21 | 2.49 | 3.03 | 3.26 | 3.75 | | |
| Ta | 1.75 | 0.902 | 0.664 | 1.32 | 0.673 | 0.965 | 0.925 | 4.10 | 1.21 | 1.01 | 0.67 | 0.77 | 0.72 | 0.67 | 0.52 | | |
| Pb | 62.6 | 22.6 | 267 | 18.6 | 38 | 162 | 103 | 12.4 | 17.71 | 18.70 | 16.66 | 16.08 | 17.08 | 18.15 | 21.01 | | |
| Th | 11.6 | 10.2 | 7.94 | 13.2 | 7.83 | 11.4 | 13.1 | 36.2 | 25.98 | 38.59 | 13.99 | 16.76 | 19.87 | 15.63 | 18.38 | | |
| La | 28.3 | 28.4 | 30.7 | 33.7 | 26 | 38.4 | 36.7 | 40.1 | 32.93 | 38.41 | 18.56 | 24.27 | 25.59 | 19.73 | 18.77 | | |
| Ce | 56.2 | 62.4 | 64.3 | 71 | 49.2 | 74.3 | 70.7 | 71.9 | 64.48 | 75.64 | 36.39 | 48.26 | 49.69 | 39.11 | 37.98 | | |
| Pr | 6.38 | 7.23 | 7.1 | 8.21 | 5.55 | 8.23 | 8.01 | 7.47 | 7.58 | 8.61 | 4.24 | 5.63 | 5.74 | 4.56 | 4.42 | | |
| Nd | 23.9 | 27.9 | 26.9 | 31.3 | 20.9 | 30.7 | 29.9 | 28.1 | 29.42 | 32.73 | 16.37 | 21.78 | 22.10 | 17.44 | 17.16 | | |
| Sm | 4.82 | 5.56 | 5.22 | 6.13 | 3.88 | 5.8 | 5.64 | 5.48 | 5.91 | 6.23 | 3.34 | 4.35 | 4.26 | 3.51 | 3.33 | | |
| Eu | 1.06 | 1.18 | 1.04 | 1.19 | 0.83 | 1.16 | 1.08 | 1.02 | 0.92 | 0.93 | 0.65 | 0.74 | 0.73 | 0.64 | 0.59 | | |
| Gd | 4.67 | 4.85 | 4.62 | 5.22 | 3.38 | 4.98 | 4.78 | 4.71 | 5.49 | 5.61 | 3.23 | 3.75 | 3.79 | 3.33 | 3.15 | | |
| Tb | 0.79 | 0.75 | 0.71 | 0.83 | 0.54 | 0.77 | 0.75 | 0.76 | 0.81 | 0.86 | 0.51 | 0.53 | 0.55 | 0.52 | 0.46 | | |
| Dy | 4.96 | 4.56 | 4.22 | 4.86 | 3.15 | 4.42 | 4.33 | 4.48 | 4.78 | 5.22 | 2.99 | 2.97 | 3.22 | 3.07 | 2.65 | | |
| Ho | 1.02 | 0.96 | 0.86 | 1 | 0.66 | 0.89 | 0.90 | 0.90 | 0.97 | 1.08 | 0.59 | 0.56 | 0.63 | 0.63 | 0.51 | | |
| Er | 2.89 | 2.76 | 2.42 | 2.86 | 1.91 | 2.56 | 2.61 | 2.51 | 2.89 | 3.35 | 1.72 | 1.59 | 1.83 | 1.82 | 1.47 | | |
| Tm | 0.42 | 0.4 | 0.35 | 0.42 | 0.28 | 0.38 | 0.39 | 0.36 | 0.42 | 0.51 | 0.25 | 0.23 | 0.27 | 0.27 | 0.21 | | |

| | | | | | | | | | | | | | | | |
|---|---|---|---|---|---|---|---|---|---|---|---|---|---|---|---|
| Yb | 2.77 | 2.74 | 2.37 | 2.82 | 1.89 | 2.5 | 2.63 | 2.36 | 2.75 | 3.63 | 1.56 | 1.51 | 1.72 | 1.73 | 1.41 |
| Lu | 0.41 | 0.41 | 0.36 | 0.43 | 0.28 | 0.36 | 0.40 | 0.35 | 0.39 | 0.55 | 0.22 | 0.23 | 0.24 | 0.23 | 0.2 |

Table S4 Principal-components analysis results for the rare earth element (REE) ratios. Based on the best coefficients for PC1 (values > 0.80) and PC2 (values > 0.60), we selected (Gd/Yb)n, (La/Yb)n, (La/Lu)n, the light to heavy REE ratio (LREE/HREE), (La/Gd)n, (La/Sm)n, (Gd/Er)n, and La/Er as fingerprints for the sample similarity analysis.

| | Initial eigenvalue | | | Component matrix | | |
|---|---|---|---|---|---|---|
| | Total | Percentage of variance (%) | Cumulative (%) | Trace elements | Coefficients of PC1 | Coefficients of PC2 |
| 1 | 5.24 | 47.69% | 47.69% | **Sc** | **0.35** | -0.24 |
| 2 | 2.87 | 26.16% | 73.85% | Rb | 0.29 | -0.35 |
| 3 | 0.95 | 8.65% | 82.50% | Sr | 0.20 | -0.37 |
| 4 | 0.64 | 5.83% | 88.33% | **Y** | **0.37** | -0.07 |
| 5 | 0.49 | 4.54% | 92.87% | **Zr** | 0.31 | 0.36 |
| 6 | 0.25 | 2.33% | 95.20% | **Nb** | **0.39** | 0.12 |
| 7 | 0.23 | 2.11% | 97.30% | Ba | 0.32 | -0.15 |
| 8 | 0.16 | 1.51% | 98.82% | **Hf** | 0.28 | 0.40 |
| 9 | 0.09 | 0.85% | 99.67% | **Ta** | **0.34** | 0.25 |
| 10 | 0.03 | 0.32% | 99.99% | Pb | 0.20 | -0.15 |
| 11 | 0 | 0.01% | 100.00% | Th | 0.01 | 0.49 |

Table S5 Principal-components (PC) analysis results for the trace element ratios and for rare earth elements (REE). Based on the best coefficients for PC1 (> 0.80), we selected the Y/REE, Y/Tb, Y/La, and Y/Nd ratios as fingerprints for the sample similarity analysis.

| | Initial eigenvalue | | | Component matrix | | |
|---|---|---|---|---|---|---|
| | Total | Percentage of variance (%) | Cumulative (%) | Trace elements | Coefficients of PC1 | Coefficients of PC2 |
| 1 | 6.45 | 43.01% | 43.01% | La/Th | -0.14 | 0.39 |
| 2 | 4.27 | 28.48% | 71.49% | Zr/Hf | 0.13 | 0.30 |
| 3 | 1.79 | 11.98% | 83.46% | Y/Nb | 0.06 | 0.07 |
| 4 | 1.37 | 9.16% | 92.62% | Nb/Ta | 0.33 | 0.05 |
| 5 | 0.50 | 3.40% | 96.02% | Sc/Y | -0.07 | 0.37 |
| 6 | 0.32 | 2.16% | 98.18% | **Y/REE** | 0.38 | 0.01 |
| 7 | 0.09 | 0.63% | 98.80% | Th/Sc | -0.01 | -0.39 |
| 8 | 0.07 | 0.51% | 99.31% | Th/REE | 0.10 | -0.44 |
| 9 | 0.04 | 0.31% | 99.62% | **Y/Yb** | 0.37 | 0.05 |
| 10 | 0.03 | 0.23% | 99.85% | **Y/Tb** | 0.38 | 0.02 |
| 11 | 0.01 | 0.09% | 99.94% | **Y/La** | 0.38 | 0.05 |
| 12 | 0 | 0.04% | 99.98% | **Y/Nd** | 0.38 | 0.04 |
| 13 | 0 | 0.01% | 99.99% | Sc/La | 0.28 | 0.22 |
| 14 | 0 | 0.01% | 100.00% | Th/Tb | 0.09 | -0.44 |
| 15 | 0 | 0.00% | 100.00% | La/Tb | -0.04 | -0.02 |

Table S6 Principal-components analysis results for the rare earth element (REE) ratios. Based on the best coefficients for PC1 (values > 0.80) and PC2 (values > 0.60), we selected (Gd/Yb)n, (La/Yb)n, (La/Lu)n, the light to heavy REE ratio (LREE/HREE), (La/Gd)n, (La/Sm)n, (Gd/Er)n, and La/Er as fingerprints for the sample similarity analysis.

| | Initial eigenvalue | | | | Component matrix | |
|---|---|---|---|---|---|---|
| | Total | Percentage of Variance (%) | Cumulative (%) | REE elements | Coefficients of PC1 | Coefficients of PC2 |
| 1 | 12.88 | 92.03% | 92.03% | **La** | 0.24 | 0.47 |
| 2 | 0.83 | 5.94% | 97.96% | **Ce** | 0.25 | 0.41 |
| 3 | 0.15 | 1.14% | 99.11% | **Pr** | 0.26 | 0.35 |
| 4 | 0.05 | 0.38% | 99.49% | **Nd** | 0.26 | 0.28 |
| 5 | 0.04 | 0.34% | 99.83% | Sm | 0.27 | 0.15 |
| 6 | 0.01 | 0.07% | 99.90% | Eu | 0.26 | -0.04 |
| 7 | 0 | 0.04% | 99.94% | Gd | 0.27 | -0.003 |
| 8 | 0 | 0.03% | 99.97% | Tb | 0.27 | -0.08 |
| 9 | 0 | 0.02% | 99.98% | Dy | 0.27 | -0.20 |
| 10 | 0 | 0.01% | 99.99% | Ho | 0.27 | -0.24 |
| 11 | 0 | 0.00% | 99.99% | Er | 0.26 | -0.26 |
| 12 | 0 | 0.00% | 100.00% | Tm | 0.26 | -0.27 |
| 13 | 0 | 0.00% | 100.00% | Yb | 0.26 | -0.25 |
| 14 | 0 | 0.00% | 100.00% | Lu | 0.26 | -0.23 |

Table S7 Principal-components analysis results for the rare earth element (REE) ratios. Based on the best coefficients for PC1 (values > 0.80) and PC2 (values > 0.60), we selected (Gd/Yb)n, (La/Yb)n, (La/Lu)n, the light to heavy REE ratio (LREE/HREE), (La/Gd)n, (La/Sm)n, (Gd/Er)n, and La/Er as fingerprints for the sample similarity analysis.

| | Initial eigenvalue | | | | Component matrix | |
|---|---|---|---|---|---|---|
| | Total | Percentage of Variance (%) | Cumulative (%) | REE elements | Coefficients of PC1 | Coefficients of PC2 |
| 1 | 6.64 | 55.38% | 55.38% | Eu/Eu* | -0.20 | 0.21 |
| 2 | 1.84 | 15.36% | 70.74% | δCe | -0.09 | -0.34 |
| 3 | 1.57 | 13.08% | 83.82% | (Gd/Yb)n | 0.28 | -0.34 |
| 4 | 0.90 | 7.57% | 91.40% | **(La/Yb)n** | 0.37 | 0.01 |
| 5 | 0.77 | 6.43% | 97.83% | **(La/Sm)n** | 0.27 | 0.46 |
| 6 | 0.14 | 1.21% | 99.03% | **(La/Lu)n** | 0.37 | 0.03 |
| 7 | 0.07 | 0.60% | 99.63% | **LREE/HREE** | 0.35 | -0.01 |
| 8 | 0.03 | 0.31% | 99.94% | **(La/Gd)n** | 0.05 | 0.39 |
| 9 | 0 | 0.03% | 99.97% | **(Gd/Er)n** | 0.30 | -0.37 |
| 10 | 0 | 0.02% | 99.99% | **La/Er** | 0.37 | 0.02 |
| 11 | 0 | 0.01% | 100.00% | Eu/Sm | -0.23 | 0.23 |
| 12 | 0 | 0.00% | 100.00% | Nd/Sm | 0.28 | 0.37 |

Figure S1 (a) Spatial distribution of the sample sites shown in Table 1, sample names used at each site, and locations of the weather stations. Site abbreviations: A, Alxa Plateau; C; Hexi Corridor Desert; G, Guerbantonggute Desert; H, Heihe River Basin; L, Lanzhou; M, Mu Us Desert; Q, Qaidam Basin Desert; T, Tengger Desert. (b) Atmospheric dust sampler used in this study.

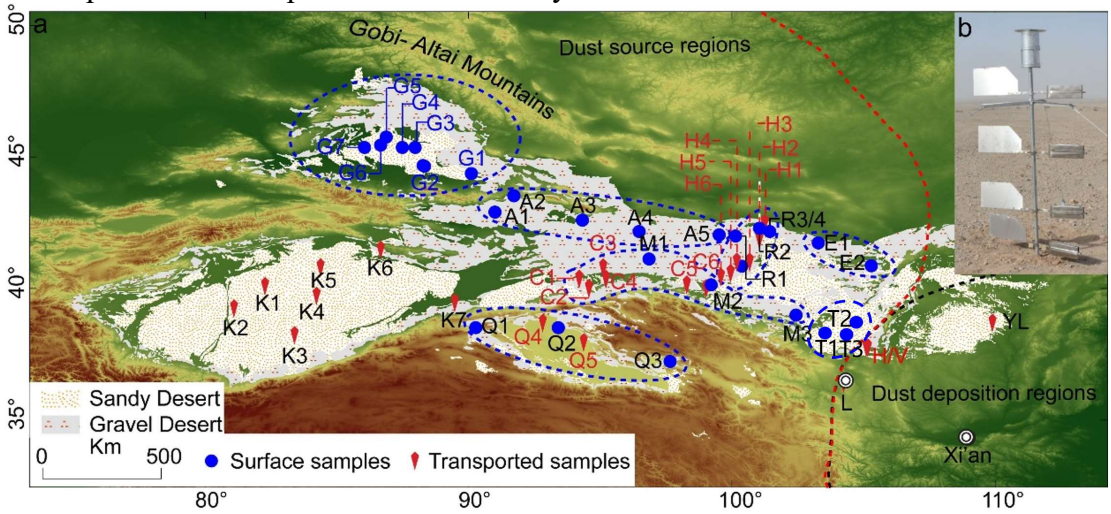


## Supplemental References


Bird, A., Stevens, T. , Rittner, M., et al., 2015. Quaternary dust source variation across the Chinese Loess Plateau. Palaeogeogr. Palaeoclimatol. Palaeoecol., 435, 254–264.

Chen, J., Li, G., Yang, J., Rao, J., Lu, H., Balsam, W., Sun, Y., Ji, J., 2007. Nd and Sr isotopic characteristics of Chinese deserts: implications for the provenances of Asian dust. Geochimica et Cosmochimica Acta, 71, 3904–3914.

Chen, X.L., Song, Y.G., Li, J.C., et al., 2017. Size-differentiated REE characteristics and environmental significance of aeolian sediments in the Ili Basin of Xinjiang, NW China. Journal of Asian Earth Sciences, 143, 30–38.

Dong, Z.B., Ping Lv, Zhengcai Zhang, Junfeng Lu. Aeolian transport over a developing transverse dune. Journal of Arid Land, 2014, 6(3): 243–254.

Ding, Z.L., Sun, J.M., Yang, S.L., et al., 2001. Geochemistry of the Pliocene red clay formation in the Chinese Loess Plateau and implications for its origin, source provenance and paleoclimate change. Geochimica et Cosmochimica Acta, 65, 901–913.

Ferrat, M., Weiss, D.J., Strekopytov, S., Dong, S.F., Chen, H.Y., Najorka, J., Sun, Y.B., Gupta, S., Tada, R., Sinha, R., 2011. Improved provenance tracing of Asian dust sources using rare earth elements and selected trace elements for palaeomonsoon studies on the eastern Tibetan Plateau. Geochimica et Cosmochimica Acta, 75, 6374–6399.

Fryberger, S.G., Dean, G., 1979. Dune forms and winds regime. McKee E D. A study of global sand seas. U.S. Geological Survey. US Washington: Geological Survey Professional Paper, 137–169.

Gallet, S., Jahn, B., Torii, M., 1996. Geochemical characterization of the Luochuan loess-paleosol sequence, China, and paleoclimatic implications Chemical Geology, 133, 67–88.

Jahn, B.M., Gallet, S., Han, J.M., 2001. Geochemistry of the Xining, Xifeng and Jixian

sections, Loess Plateau of China: eolian dust provenance and paleosol evolution during the last 140 ka. Chemical Geology 178, 71–94.

Kapp, P., Pelletier, J.D., Rohrmann, A., et al., 2011, Wind erosion in the Qaidam basin, central Asia: Implications for tectonics, paleoclimate, and the source of the Loess plateau: GSA Today, 21(4), 4–10.

Licht, A., Pullen, A., Kapp, P., et al., 2016. Aeolian cannibalism: reworked loess as the main sediment source of the Chinese Loess Plateau. GSA Bull, 128, 944–956.

Liu, C.Q., Masuda, A., Okada, A., Yabuki, S., Zhang, J., Fan, Z.L., 1993. A geochemical study of loess and desert sand in northern China: Implications for continental crust weathering and composition. Chem. Geol. 106, 359–374.

Liu, C.Q., Masuda, A., Okada, A., et al., 1994. Isotope geochemistry of Quaternary deposits from the arid lands in northern China. Earth and Planetary Science Letters, 127, 25–38.

Liu, Q.Q., Yang, X.P., 2018. Geochemical composition and provenance of aeolian sands in the Ordos Deserts, northern China. Geomorphology, 318, 354-374.

Maher, B.A., Mutch, T.J., Cunningham, D., 2009. Magnetic and geochemical characteristics of Gobi Desert surface sediments: Implications for provenance of the Chinese Loess Plateau. Geology, 37(3), 279–282.

Rittner, M., Vermeesch, P., Carter, A., Bird, A., Stevens, T., Garzanti, E., Andò, S., Vezzoli, G., Dutt, R., Xu, Z.W., Lu, H.Y., 2016. The provenance of Taklamakan desert sand. Earth and Planetary Science Letters, 437, 127–13.

Stevens, T., Carter, A., Watson, T.P., Vermeesch, P., Andò, S., Bird, A., Lu, H.Y., Garzanti, E., Cottam, M.A., Sevastjanova, I., 2013. Genetic linkage between the Yellow River, the Mu Us desert and the Chinese Loess Plateau. Earth-Sci. Rev. 78(15), 355–368.

Sun, J.M., 2002, Provenance of loess material and formation of loess deposits on the Chinese Loess Plateau. Earth and Planetary Science Letters, 203, 845–859.

Sun, J.M., Ding, Z.L., Xia, X.P., et al., 2018. Detrital zircon evidence for the ternary sources of the Chinese Loess Plateau. Journal of Asian Earth Science, 155, 21–34.

Wei, T., Dong, Z.W., Kang, S.C.,Qin, X., Guo, Z., 2017. Geochemical evidence for sources of surface dust deposited on the Laohugou glacier, Qilian Mountains. Appllied Geochemical, 79, 1-8.

Xie, Y.Y., Chi, Y.P., 2016. Geochemical investigation of dry- and wet-deposited dust during the same dust-storm event in Harbin, China: Constraint on provenance and implications for formation of aeolian loess. Journal of Asian Earth Science, 120, 43-61.

Yang, X., Liu, Y., Li, C., et al., 2007. Rare earth elements of aeolian deposits in Northern China and their implications for determining the provenance of dust storms in Beijing. Geomorphology, 87, 365–377.

Zhang, Z.C., Dong, Z.B., Li, C.X., 2015. Wind regime and sand transport in China's Badain Jaran Desert. Aeolian Res., 17, 1–13.